

Hydrothermal synthesis, structure and characterization of new NASICON related potassium iron (III) pyrophosphate

G S GOPALAKRISHNA[†], B H DORESWAMY, M J MAHESH[†], M MAHENDRA, M A SRIDHAR, J SHASHIDHARA PRASAD* and K G ASHAMANJARI[†]

Department of Studies in Physics, [†]Department of Studies in Geology, University of Mysore, Mysore 570 006, India

MS received 1 December 2003; revised 18 December 2004

Abstract. A new potassium iron (III) pyrophosphate was synthesized by hydrothermal technique and characterized by X-ray studies. The compound crystallizes in a monoclinic space group, $P2_1/c$, with cell parameters, $a = 7.365(2)$ Å, $b = 10.017(2)$ Å, $c = 8.214(1)$ Å, $\beta = 106.50(1)^\circ$ and $Z = 4$. The structure has tunnel-type cavities and are congenial for ion transportation through them. The compound exhibits moderate thermal stability.

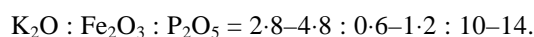
Keywords. Hydrothermal; crystal structure; solid electrolyte; iron (III) pyrophosphate.

1. Introduction

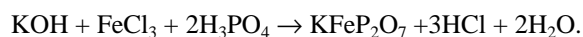
NASICON and related compounds belong to the well known family of solid electrolyte with high ionic conductivity and general formula, $\text{Na}_{1+x} \text{Zr}_2 \text{Si}_x \text{P}_{3-x} \text{O}_{12}$, with $0 < x < 3$ (Goodenough *et al* 1976; Hong 1976). The application of these materials as solid electrolytes to replace the conventional *b*-aluminas in Na batteries was initially suggested. However, NASICON-based cells are not stable when they are in contact with molten Na electrodes (Gordon *et al* 1981). However, possible application of NASICON related in Na, K or Co, Fe sensors was demonstrated and a NASICON based commercial CO_2 sensor has already been proposed (Caneiro *et al* 1991; Miura *et al* 1992; Fuentes *et al* 2001). Recently, this family of materials has attracted the attention of researchers looking for ion-selective electrodes or gas sensor devices (Ahmad *et al* 1995; Khireddine *et al* 1997; Fuentes *et al* 2001). Most of these stable ones assess the relation between composition, structure and electrical conductivity and the higher values of conductivity, and is also related to monoclinic symmetry, when x lies in the range 1.8–2.2. For other values of x , the structural modification to rhombohedral symmetry is associated with decrease in conductivity. Earlier reports indicate the use of iron phosphates with different substitutions as luminescence materials (Sarver *et al* 1961; Looeny and Brown 1971; Donker *et al* 1989; Pelova *et al* 1995). A new structural diversity of the simple stoichiometric composition of iron pyrophosphate compound (KFeP_2O_7) is reported here. The compound has been synthesized by hydrothermal technique and characterized by X-ray diffraction method.

2. Experimental

NASICON related new potassium iron (III) pyrophosphates were synthesized by the hydrothermal technique at relatively moderate temperature and pressure conditions. The growth of phosphates by hydrothermal method is relatively new. The use of hydrothermal method is quite complicated for these compounds, because of the highly corrosive and volatile nature of phosphorus at higher temperatures. The present experiments were carried out in Morey autoclaves (figure 1) provided with Teflon liners at 260°C and in the pressure range 60–100 bars. The starting materials such as iron (III) chloride and known quantity of 85% H_3PO_4 were added to the reaction vessel. The alkaline component, KOH, was added in the form of molar solution and this solution acts as a mineralizer. KFeP_2O_7 crystals could be synthesized under the following ratios



The following reactions could explain the synthesis of the compound



The experiments were carried out for 10 days and quenched to ambient conditions and thoroughly washed with distilled water. The crystals thus obtained were of good quality with well developed morphology. The morphology of the crystals varied according to the growth techniques, the physico-chemical conditions and the composition and concentration of the starting materials. On the whole, KFeP_2O_7 crystals obtained by the hydrothermal methods were of good quality and exhibited smooth surface morphology, translucent luster, gray colour; growth steps were observed to have a size in the range 0.5–3 mm (figure 2). Twinning was almost absent.

*Author for correspondence (jsp@uomphysics.net)

A prism shaped crystal with approximate size, $0.2 \times 0.2 \times 0.2$ mm, was chosen for X-ray diffraction study. The measurements were made on a DIPLabo Imaging Plate system with graphite monochromated radiation (MoK_α). Thirtysix frames of data were collected by oscillation method. Successive frames were scanned in steps of $5^\circ/\text{min}$ with an oscillation range of 5° . Lorentz and polarization corrections were applied. Image processing and data reduction were done using Denzo (Otwinowski and Minor 1997; Mackay *et al* 1999). All frames could be indexed with a monoclinic primitive lattice. The phase set with the highest combined figure of merit gave the positions of all the non-hydrogen atoms. Least-squares refinement using SHELXL-97 (Sheldrick 1997) with isotropic temperature factors for all the non-hydrogen atoms converged the residual to $R1 = 0.1453$. Few more final cycles of full-matrix least square refinement based on 934 observed reflections and 100 variable parameters with

anisotropic thermal parameters for nonhydrogen atoms and isotropic thermal parameters for hydrogen atoms converged the residual to $R1 = 0.0729$ and $wR2 = 0.2060$ and G.O.F. on F^2 was 1.108.

3. Results and discussion

The details of crystal data and refinement are given in table 1. The final positional coordinates with equivalent isotropic temperature factors and anisotropic thermal parameters (U_{ij}) of all the atoms are listed in tables 2 and 3. Bond distances and angles are given in tables 4 and 5, respectively. The bond distances and angles are in good agreement with the standard values. Figure 3 represents the ORTEP of the molecules with thermal ellipsoids at 50% probability (Johnson 1976). The packing of molecules along a and c axes exhibits a three-dimensional open framework structure with tunnel type cavities inside it (figures 4 and 5). These cavities help the movement of ions and thus support the ion transport phenomenon.

FTIR-spectrum was registered for KFeP_2O_7 compound using a high resolution Perkin Elmer Infrared Spectrophotometer in the range $4000\text{--}400\text{ cm}^{-1}$ (figure 6). This compound exhibits prominent multiple absorption bands especially in the frequency ranges 2351 cm^{-1} and $1050\text{--}459\text{ cm}^{-1}$ regions. The multiplication and fineness of the

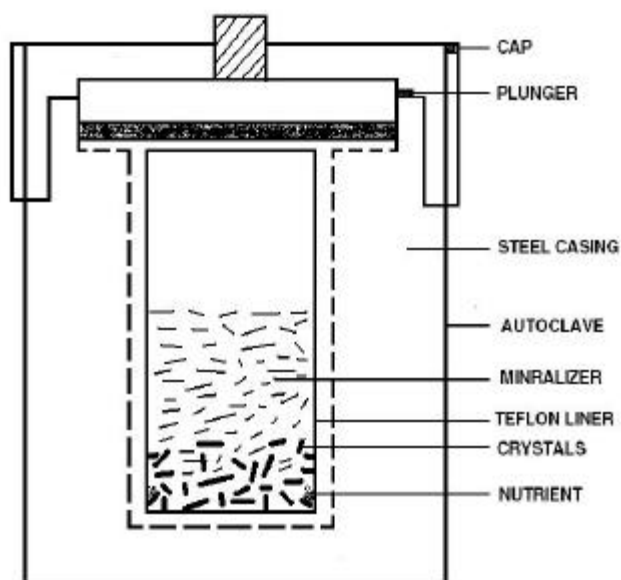


Figure 1. Schematic diagram of autoclaves.

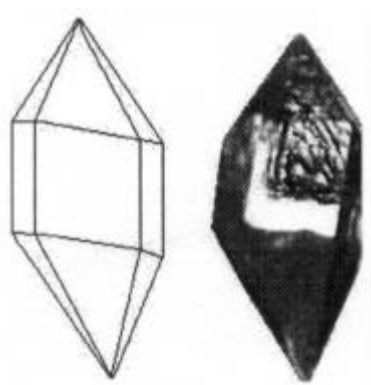


Figure 2. Growth morphology of KFeP_2O_7 .

Table 1. Crystal data and experimental details.

Empirical formula	KFeP_2O_7
Formula weight	268.89
Temperature	293(2) K
Wavelength	0.71069 \AA
Crystal system	monoclinic
Space group	$P2_1/c$ (No. 14)
Cell dimensions	$a = 7.365(2) \text{ \AA}$ $b = 10.017(2) \text{ \AA}$ $c = 8.214(1) \text{ \AA}$ $\beta = 106.50(1)^\circ$
Volume	$581.08(18) \text{ \AA}^3$
Z	4
Density (calculated)	3.074 Mg/m^3
Absorption coefficient	3.846 mm^{-1}
F_{000}	524
Crystal colour, habit	Transparent prism
Crystal size	$0.2 \times 0.2 \times 0.2 \text{ mm}$
Theta range for data collection	25.69° to 32.48°
Index ranges	$0 \leq h \leq 11$ $0 \leq k \leq 15$ $-12 \leq l \leq 11$
Reflections collected	1054
Independent reflections	1007 [R (int) = 0.0478]
Observation data [$I > 2s(I)$]	934
Refinement method	Full-matrix least-squares
Data/restraints/parameters	1007/0/100
Goodness-of-fit on F^2	1.108
Final R indices [$I > 2s(I)$]	$R1 = 0.0729$, $wR2 = 0.2060$
R indices (all data)	$R1 = 0.0753$, $wR2 = 0.2100$
Largest diff. peak and hole	1.292 and $-1.598 \text{ e. \AA}^{-3}$

Table 2. Atomic coordinates and equivalent thermal parameters.

Atom	x	y	z	U_{eq}
Fe1	0.76443(8)	0.59977(5)	0.23977(8)	0.0054(8)
P3	0.86611(16)	0.90457(10)	0.16990(14)	0.0059(8)
P7	0.44223(14)	0.36295(10)	0.19036(14)	0.0055(8)
O9	0.3218(7)	0.3922(4)	0.0127(5)	0.0160(10)
O2	0.8542(7)	0.9106(5)	− 0.0147(5)	0.0155(10)
O6	0.6594(5)	0.9406(3)	0.1872(5)	0.0093(9)
O10	0.4527(5)	0.2160(3)	0.2417(5)	0.0101(9)
O8	0.6404(5)	0.4203(4)	0.2309(5)	0.0120(10)
O5	0.9183(5)	0.7665(4)	0.2458(5)	0.0104(9)
O4	0.9984(5)	1.0074(3)	0.2778(4)	0.0087(9)
K11	0.82174(16)	0.17961(13)	0.44652(15)	0.0189(8)

Table 3. Anisotropic thermal parameters.

Atom	U_{11}	U_{22}	U_{33}	U_{12}	U_{13}	U_{23}
Fe1	0.0066(8)	0.0012(8)	0.0067(8)	0.00010(13)	− 0.0010(3)	− 0.00020(13)
P3	0.0075(9)	0.0023(9)	0.0062(9)	− 0.0015(3)	− 0.0006(4)	− 0.0002(3)
P7	0.0063(8)	0.0018(8)	0.0072(9)	− 0.0006(3)	− 0.0002(4)	0.0004(3)
O9	0.0191(18)	0.0156(17)	0.0078(16)	0.0006(12)	− 0.0050(12)	0.0019(10)
O2	0.0186(17)	0.0211(18)	0.0058(15)	− 0.0100(13)	0.0018(12)	− 0.0018(11)
O6	0.0078(14)	0.0064(14)	0.0133(14)	0.0034(9)	0.0026(9)	0.0045(9)
O10	0.0086(13)	0.0026(14)	0.0165(15)	− 0.0006(9)	− 0.0006(10)	0.0015(10)
O8	0.0093(14)	0.0050(13)	0.0203(17)	− 0.0032(9)	0.0020(11)	0.0017(10)
O5	0.0107(14)	0.0020(13)	0.0162(15)	0.0016(8)	0.0001(10)	− 0.0001(9)
O4	0.0107(15)	0.0038(12)	0.0097(14)	− 0.0041(9)	− 0.0001(9)	− 0.0031(9)
K11	0.0180(9)	0.0183(9)	0.0166(9)	0.0020(3)	− 0.0013(4)	0.0008(3)

Table 4. Bond lengths (Å).

Atoms	Length	Atoms	Length
Fe(1)–O(2)#1	1.938(4)	P(7)–O(10)	1.527(4)
Fe(1)–O(9)#2	1.991(4)	P(7)–O(6)#9	1.614(4)
Fe(1)–O(8)	2.008(4)	P(7)–K(11)	3.5031(16)
Fe(1)–O(5)	2.012(4)	P(7)–K(11)#4	3.7235(17)
Fe(1)–O(4)#3	2.017(3)	O(9)–K(11)#4	3.118(5)
Fe(1)–O(10)#4	2.019(3)	O(2)–K(11)#6	3.257(5)
Fe(1)–K(11)#5	3.7935(15)	O(6)–K(11)#8	3.202(4)
P(3)–O(2)	1.495(4)	O(10)–K(11)	2.785(4)
P(3)–O(4)	1.518(3)	O(8)–K(11)	3.064(4)
P(3)–O(5)	1.521(4)	O(8)–K(11)#5	3.164(5)
P(3)–O(6)	1.610(4)	O(5)–K(11)#7	2.756(4)
P(3)–K(11)#7	3.4362(17)	O(5)–K(11)#6	2.939(4)
P(3)–K(11)#6	3.5395(18)	O(4)–Fe(1)#6	2.017(3)
P(3)–K(11)#8	3.6445(18)	O(4)–K(11)#8	2.760(4)
P(7)–O(9)	1.505(4)	O(4)–K(11)#7	2.947(4)
P(7)–O(8)	1.515(4)		

Symmetry transformations used to generate equivalent atoms:
 [#1 $x, -y + 3/2, z + 1/2$, #2 $-x + 1, -y + 1, -z$, #3 $-x + 2, y - 1/2, -z + 1/2$, #4 $-x + 1, y + 1/2, -z + 1/2$, #5 $x, -y + 1/2, z - 1/2$, #6 $-x + 2, y + 1/2, -z + 1/2$, #7 $-x + 2, -y + 1, -z + 1$, #8 $x, y + 1, z$, #9 $-x + 1, y - 1/2, -z + 1/2$, #10 $x, -y + 3/2, z - 1/2$, #11 $x, y - 1, z$ and #12 $x, -y + 1/2, z + 1/2$]

Table 5. Bond angles ($^{\circ}$).

Atoms	Angle	Atoms	Angle
O(2)#1–Fe(1)–O(9)#2	178.51(19)	P(7)–O(8)–K(11)	93.61(17)
O(2)#1–Fe(1)–O(8)	90.40(19)	Fe(1)–O(8)–K(11)	124.35(16)
O(2)#1–Fe(1)–O(5)	89.75(18)	P(7)–O(8)–K(11)#5	107.5(2)
O(8)–Fe(1)–O(5)	172.56(15)	Fe(1)–O(8)–K(11)#5	91.55(14)
O(2)#1–Fe(1)–O(4)#3	90.19(15)	K(11)–O(8)–K(11)#5	88.38(11)
O(9)#2–Fe(1)–O(4)#3	88.32(17)	P(3)–O(5)–Fe(1)	132.1(2)
O(5)–Fe(1)–O(4)#3	83.65(14)	P(3)–O(5)–K(11)#7	103.11(17)
O(2)#1–Fe(1)–O(10)#4	89.78(15)	Fe(1)–O(5)–K(11)#7	115.15(16)
O(9)#2–Fe(1)–O(10)#4	91.71(18)	P(3)–O(5)–K(11)#6	100.17(18)
O(5)–Fe(1)–O(10)#4	88.38(14)	Fe(1)#6–O(4)–K(11)#8	106.90(13)
O(2)#1–Fe(1)–K(11)#5	123.67(12)	P(3)–O(4)–K(11)#7	95.22(16)
O(5)–Fe(1)–K(11)#5	117.70(11)	Fe(1)#6–O(4)–K(11)#7	97.89(13)
O(10)#4–Fe(1)–K(11)#5	134.98(10)	O(5)#7–K(11)–O(10)	146.40(12)
O(2)#1–Fe(1)–K(11)#6	110.42(15)	O(4)#11–K(11)–O(10)	107.30(11)
O(8)–Fe(1)–K(11)#6	124.95(12)	O(5)#7–K(11)–O(5)#3	92.64(10)
O(10)#4–Fe(1)–K(11)#6	129.90(11)	O(10)–K(11)–O(5)#3	108.04(11)
O(2)–P(3)–O(4)	114.0(2)	O(4)#11–K(11)–O(4)#7	79.36(11)
O(2)–P(3)–O(5)	112.8(2)	O(10)–K(11)–O(4)#7	134.10(11)
O(4)–P(3)–O(5)	109.39(19)	O(5)#3–K(11)–O(4)#7	112.47(10)
O(2)–P(3)–O(6)	107.2(2)	O(5)#7–K(11)–O(8)	116.82(11)
O(4)–P(3)–O(6)	105.2(2)	O(5)#3–K(11)–O(8)	72.52(11)
O(5)–P(3)–O(6)	107.65(19)	O(4)#7–K(11)–O(8)	166.19(12)
O(2)–P(3)–K(11)#7	140.4(2)	O(5)#7–K(11)–O(9)#9	104.52(11)
O(4)–P(3)–K(11)#7	58.67(14)	O(10)–K(11)–O(9)#9	83.29(11)
O(6)–P(3)–K(11)#7	112.17(14)	O(5)#3–K(11)–O(9)#9	128.61(12)
O(4)–P(3)–K(11)#6	103.36(15)	O(8)–K(11)–O(9)#9	133.10(11)
O(6)–P(3)–K(11)#6	150.44(13)	O(4)#11–K(11)–O(8)#12	122.08(11)
O(5)–P(3)–K(11)#8	119.26(15)	O(10)–K(11)–O(8)#12	86.74(11)
O(6)–P(3)–K(11)#8	61.37(13)	O(5)#3–K(11)–O(8)#12	165.12(10)
K(11)#7–P(3)–K(11)#8	76.64(4)	O(5)#7–K(11)–O(6)#11	141.94(10)
K(11)#6–P(3)–K(11)#8	146.09(4)	O(8)–K(11)–O(6)#11	100.64(10)
O(9)–P(7)–O(8)	113.9(3)	O(10)–K(11)–O(2)#3	123.56(11)
O(9)–P(7)–O(10)	115.2(2)	O(4)#7–K(11)–O(2)#3	99.91(10)
O(8)–P(7)–O(10)	109.6(2)	O(8)–K(11)–O(2)#3	73.63(11)
O(8)–P(7)–O(6)#9	105.6(2)	O(9)#9–K(11)–O(2)#3	153.13(12)
O(9)–P(7)–K(11)	146.51(19)	O(6)#11–K(11)–O(2)#3	139.71(10)
O(8)–P(7)–K(11)	60.81(15)	O(4)#11–K(11)–P(3)#7	91.08(8)
O(10)–P(7)–K(11)	50.19(13)	O(10)–K(11)–P(3)#7	150.47(9)
O(6)#9–P(7)–K(11)	108.10(14)	O(5)#3–K(11)–P(3)#7	101.38(8)
O(8)–P(7)–K(11)#4	97.53(15)	O(8)–K(11)–P(3)#7	142.30(8)
P(7)–O(9)–Fe(1)#2	160.7(3)	O(9)#9–K(11)–P(3)#7	80.44(8)
P(7)–O(9)–K(11)#4	101.5(2)	O(6)#11–K(11)–P(3)#7	116.92(7)
P(3)–O(2)–Fe(1)#10	163.2(3)	O(2)#3–K(11)–P(3)#7	75.52(8)
P(3)–O(2)–K(11)#6	88.2(2)	O(5)#7–K(11)–P(7)	132.54(9)
Fe(1)#10–O(2)–K(11)#6	99.07(18)	O(4)#11–K(11)–P(7)	115.83(8)
P(3)–O(6)–P(7)#4	124.4(2)	O(5)#3–K(11)–P(7)	92.99(8)
P(3)–O(6)–K(11)#8	92.44(14)	O(4)#7–K(11)–P(7)	154.47(8)
P(7)#4–O(6)–K(11)#8	95.60(17)	O(8)–K(11)–P(7)	25.57(7)
P(7)–O(10)–K(11)	104.90(16)	O(9)#9–K(11)–P(7)	108.15(9)
Fe(1)#9–O(10)–K(11)	122.49(15)	O(2)#3–K(11)–P(7)	98.72(8)

absorption bands of phosphates lie in the lower range, which indicates complexity of the internal crystalline structure of the $[\text{PO}_4]$ tetrahedron. The degree of condensation of the anion, $[\text{PO}_4]^{3-}$ to $[\text{P}_2\text{O}_7]^{4-}$, is directly related to its multiplicity of absorption bands (Byrappa *et al* 1970). This compound has relatively more bands in the medium to low frequency region, i.e. $906\text{--}459\text{ cm}^{-1}$, when compared to earlier reported pyrophosphate compound (Gopalakrishna *et al* 2001). The degree of condensation of phos-

phate is observed in the latter region and is also confirmed by X-ray studies.

To provide more information on the mechanism of the formation of KFeP_2O_7 crystals, we have carried out differential thermal study on the compounds. The DTA curve was recorded for KFeP_2O_7 using DTA/ETA instrument (Model 021 NAL India) from room temperature to 500°C . The results yielded multiple phase transitions at 180, 428 and 480°C (figure 7). The preliminary impedance

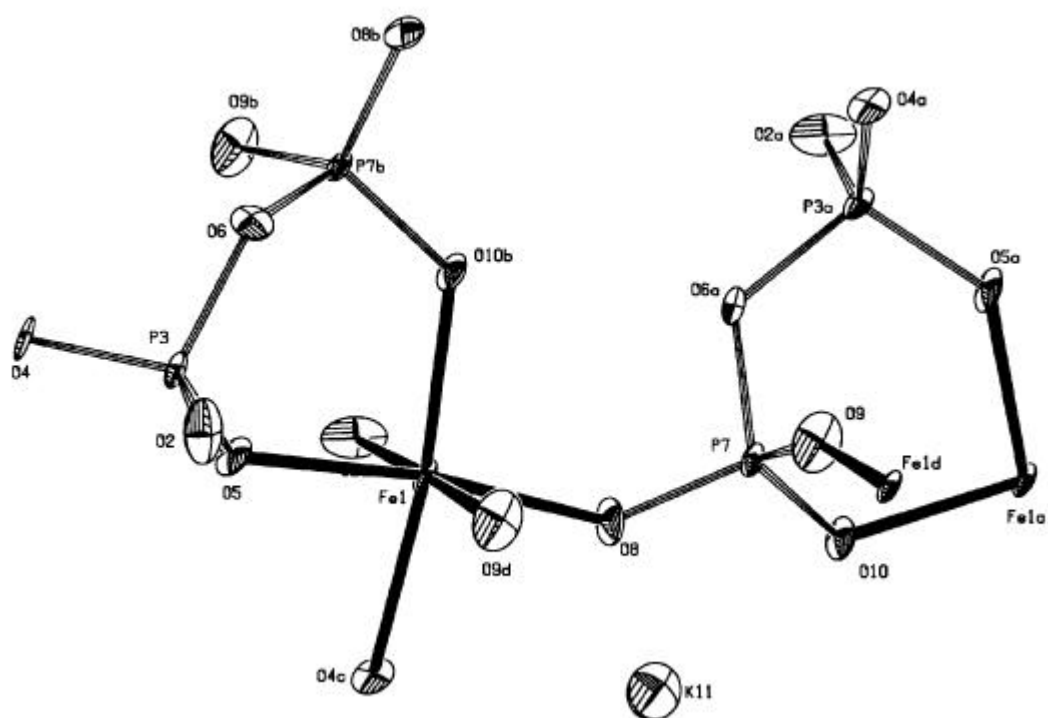


Figure 3. Perspective diagram of the molecule with thermal ellipsoids at 50% probability [Symmetry codes: $a = (1 - x, -1/2 + y, 1/2 - z)$, $b = (1 - x, 1/2 + y, 1/2 - z)$, $c = (2 - x, -1/2 + y, 1/2 - z)$, $d = (1 - x, 1 - y, -z)$ and $e = (x, 3/2 - y, 1/2 + z)$].

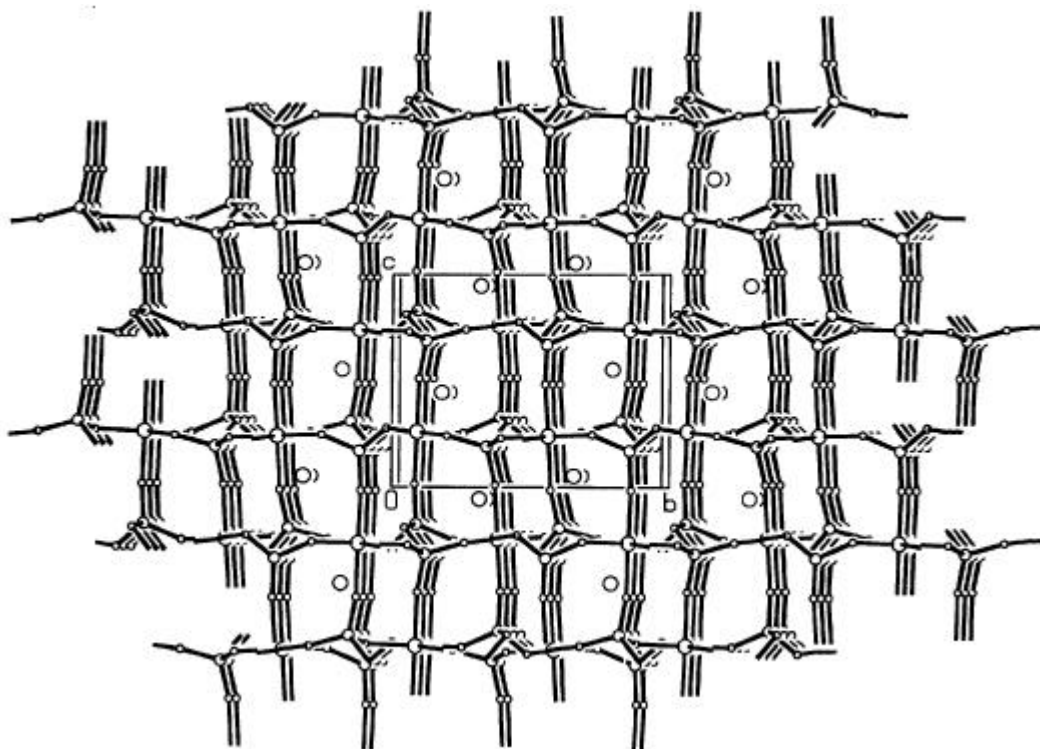


Figure 4. Packing of the molecules down a -axis.

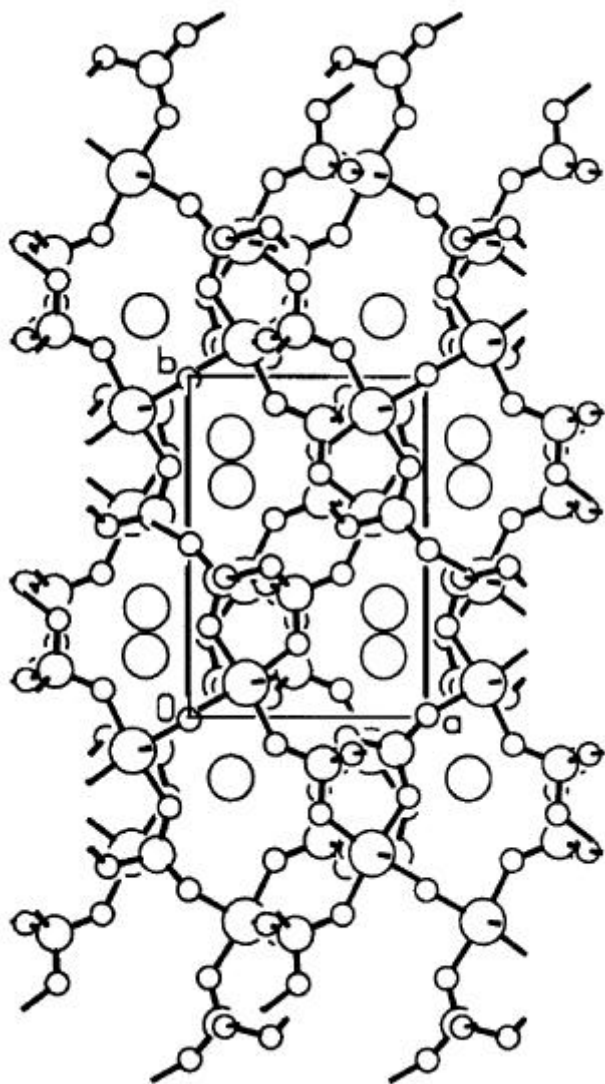


Figure 5. Packing of the molecules down c -axis.

spectroscopy results are encouraging. Ionic conductivity values of this compound are of the order of 10^{-6} to $10^{-4} \Omega \text{ cm}^{-1}$ at 573 K. Detailed impedance spectroscopy studies are under way.

4. Conclusions

KFeP_2O_7 crystals synthesized by hydrothermal method in the form of single crystals have well developed morphology. Single crystal structural study of this monoclinic compound reveals that it has an open-framework tunnel type cavity structure.

Acknowledgements

The authors would like to express their thanks to DST, New Delhi, for financial assistance under the projects SP/S2/M-44/96-97 and SP/I2/FOO/93.

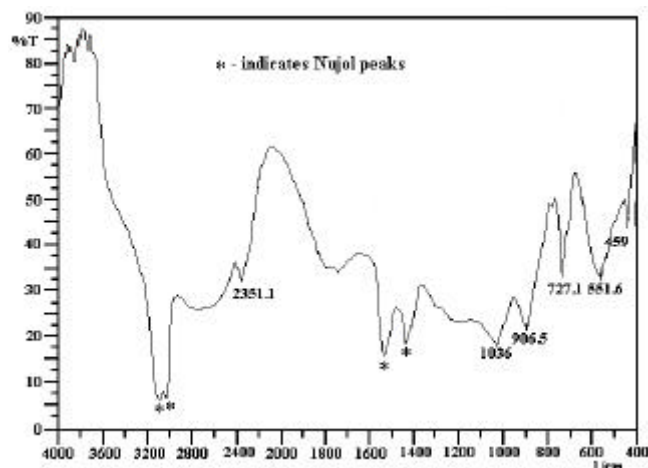


Figure 6. Infrared spectra of KFeP_2O_7 .

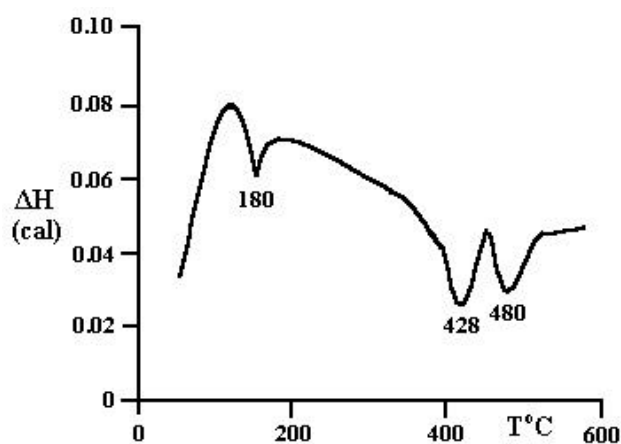


Figure 7. DTA curve.

References

- Ahmad A, Glasgow C and Wheat T A 1995 *Solid State Ionics* **76** 143
- Byrappa K, Plysnnina I I and Dorohova G I 1970 *J. Electroanalit. Chem.* **74** 125
- Caneiro A, Fabry P, Hireddine H K and Siebert E 1991 *Anal. Chem.* **63** 2550
- Donker H, Smit W A and Blasse G 1989 *J. Electrochem. Soc.* **136** 3130
- Fuentes R O, Figueiredo F M, Marques F M B and Franco J I 2001a *Solid State Ionics* **139** 309
- Fuentes R O, Figueiredo F M, Marques F M B and Franco J I 2001b *Solid State Ionics* **140** 173
- Goodenough J B, Hong H Y P and Kafalas J A 1976 *Mater. Res. Bull.* **11** 203
- Gopalakrishna G S, Shashidhara Prasad J and Lokanath N K 2001 *Proc. joint 4th ISHR and 6th ICSTR* (eds) K Yanagisawa and Qi Feng (Kochi, Japan)
- Gordon R S, Miller G R, Beck E D and Rasmussen J R 1981 *Solid State Ionics* **3/4** 243
- Hong H Y P 1976 *Mater. Res. Bull.* **11** 173

- Johnson C K 1976 ORTEP-II, A Fortran Thermal-Ellipsoid Plot Program. Report ORNL-5138. Oak Ridge National Laboratory, Oak Ridge, Tennessee, USA
- Khiredine H, Fabry P, Caneiro A and Bochu B 1997 *Sens. & Actuators* **B40** 223
- Looeny J R and Brown J J 1971 *J. Electrochem. Soc.* **118** 470
- Mackay S, Gilmore C J, Edwards C, Stewart N and Shankland K 1999 *maXus Computer program for the solution and refinement of crystal structures* (The Netherlands: Bruker Nonius, Japan: MacScience and The University of Glasgow)
- Miura N, Yao S, Shimizu Y and Yamazoe N 1992 *Sens. & Actuators* **B9** 165
- Otwinowski Z and Minor W 1997 in *Methods in enzymology* (eds) C W Carter Jr. and R M Sweet (New York: Academic Press) **276** pp 307–326
- Pelova V, Kynev K and Gochev G 1995 *J. Mater. Sci. Lett.* **14** 330
- Sarver J F, Hoffman M V and Hummel F A 1961 *J. Electrochem. Soc.* **108** 1103
- Sheldrick G M 1997 *SHELXL-97, Program for the refinement of crystal structures* (Germany: University of Göttingen)